A CD45RO+ stem cell memory T cell population intermediate to canonical stem cell memory and central memory T cells in human cancer.

Daniel Powell Jr. (poda@pennmedicine.upenn.edu)
University of Pennsylvania School of Medicine https://orcid.org/0000-0002-5966-8908
Monika Eiva
University of Pennsylvania
Erica Brown
University of Pennsylvania
Veethika Pandey
University of Pennsylvania
Alexander Benton
University of Pennsylvania https://orcid.org/0000-0002-1854-2540
Stacy Thomas
University of Pennsylvania
Wenzhao Meng
University of Pennsylvania
Aaron Rosenfeld
University of Pennsylvania https://orcid.org/0000-0002-2266-0355
Eline Luning Prak
University of Pennsylvania https://orcid.org/0000-0002-9478-9211

Article

Keywords:

Posted Date: February 3rd, 2022

DOI: https://doi.org/10.21203/rs.3.rs-1296773/v1

A CD45RO+ stem cell memory T cell population intermediate to canonical stem cell memory and central memory T cells in human cancer.

Monika A. Eiva[1,2,3], Erica G. Brown[1,2,3], Veethika Pandey[1,2,3], Alexander B. Benton[1,2,3], Stacy K. Thomas[4,5], Wenzhao Meng[3], Aaron M. Rosenfeld[3], Eline T. Luning Prak[3,5], Daniel J. Powell Jr.[1,2,3,5]

1. Ovarian Cancer Research Center, Department of Obstetrics and Gynecology, Perelman School of Medicine, University of Pennsylvania, Philadelphia, PA, United States.
2. Center for Cellular Immunotherapies, Abramson Cancer Center, University of Pennsylvania, Philadelphia, PA, United States.
3. Department of Pathology and Laboratory Medicine, Perelman School of Medicine, University of Pennsylvania, Philadelphia, PA, United States
4. Division of Hematology-Oncology, Department of Medicine, Perelman School of Medicine, University of Pennsylvania, Philadelphia, PA
5. Abramson Cancer Center, Perelman School of Medicine, University of Pennsylvania, Philadelphia, PA

Correspondence should be addressed to D.J.P (poda@pennmedicine.upenn.edu)

Daniel J. Powell Jr., PhD

University of Pennsylvania

3400 Civic Center Blvd.

Bldg. 421, TRC Rm 8-103

Philadelphia, PA 19104-5156

Office: 215-573-4783

Abstract

T memory stem cells (Tscm) are integral for effective immunotherapy and antitumor responses, but little is known about Tscm immunobiology in solid human tumors. Here we identify self-renewing and multipotent Tscm tumor-infiltrating lymphocytes (TILs) in human cancer and present a novel Tscm subset which expresses CD45RO, is derived from CD45RO- Tscm T cells, and is capable of self-renewal and multipotency. From the analysis of CD45RO+ Tscm differentiation, phenotyping, gene expression, and the broader TCR repertoire, we find CD45RO+ Tscm cells are hierarchically positioned in between canonical CD45RO- Tscm cells and central memory T cells. Notably, CD45RO+ Tscm cells exhibit a gene expression profile with effector capabilities and a tumor-specific phenotype that is more similar to T cells associated with successful immunotherapy than canonical Tscm. Overall, we identify a novel Tscm subset in human cancer which has distinct phenotypic, transcriptional, and effector-like attributes that position it as an attractive subset for future research in the setting of cancer immunotherapy.

Main

T memory stem cells (Tscm), endowed with self-renewal and multipotent properties, are vital for immunity and successful immunotherapy responses[1–9]. Gattinoni et al.[6] first described canonical human Tscm cells, which express CCR7 (or CD62L), CD45RA, CD95, are CD45RO negative, and express other markers indicative of early memory[6]. Despite the important implications that Tscm cell biology has for the cancer field and immunotherapeutic treatments[10,11], the majority of Tscm cell studies are conducted using human peripheral blood T cells[6,12,13], mouse models[5,13], or expanded tumor-infiltrating lymphocytes (TIL)[14]. The few studies that have interrogated Tscm cells within tumors focus primarily on 'stem-like' T cells, without assessing whether these 'stem-like' T cells overlap with canonical Tscm cells[15]. Thus, there remains a gap in understanding the immunobiology of stem-like tumor-infiltrating lymphocytes in solid human tumors, despite early memory T cells being critical for solid tumor immunotherapeutic treatments such as immune checkpoint blockade and adoptive TIL therapies[10]. It also remains unclear whether less immunogenic human tumors, such ovarian cancer, harbor bona fide, canonical Tscm TILs capable of self-renewal and multipotency, and whether Tscm cells have hallmarks of tumor antigen specificity. We therefore hypothesized that Tscm cells with self-renewing, multipotent capabilities exist in human tumors and harbor characteristics indicative of tumor-specificity.

Since the existence of Tscm-like TILs in ovarian cancers has yet to be conclusively determined, we utilized unmanipulated, enzyme-digested tumor samples from human ovarian cancer patients and assayed for the presence of CD45RA+CCR7+CD95+ Tscm-like TILs (**Sup. Figure 1a**). Tscm-like TILs represented a mean frequency of 6.66 ± 0.84% of total CD3+ TILs, similar to the mean frequency of Tscm cells from healthy peripheral blood lymphocytes (PBL),

which was 5.125 ± 1.95% (**Sup. Figure 1b**), as reported elsewhere[6,12,13]. TCF1 is a transcription factor associated with self-renewing T cells and a hallmark of Tscm cells[16]. We found that both Tscm-like T cells from peripheral blood and tumor express higher levels of TCF1 than in effector memory (EM) and effector (EFF) subsets (**Sup. Figure 1c**). We then tested the self-renewal and multipotency capabilities of CD45RA+CCR7+CD95+ Tscm-like TILs. Tscm-like TILs self-renewed (1.61% retained Tscm-like phenotype) and differentiated into downstream central memory (CM; 5.83%), EM (79.17%), and effector/terminally-differentiated T cells (EFF/EMRA; 12.39%) (**Sup. Figure 1d,e)**. CD45RA+CCR7+CD95+ PBL T cells were similarly capable of self-renewal (11.75% retention) and multipotency (**Sup. Figure 1f)**. Thus, human ovarian tumors harbor naturally-occurring, stem-cell memory TILs that are capable of self-renewal and multipotency. These findings from unmanipulated TILs are of importance as previous studies that examined Tscm TILs in other human cancer types used either expanded TILs[14], T cells derived from peripheral blood[13], tumor tissue analysis in the absence of functional studies[5], or relied on TCF-1 as a stem-like T cell marker without combined use of CCR7, CD45RA, CD62L or other such memory markers[15].

In an examination of Tscm TIL phenotypic heterogeneity using cytometry by time of flight (CyTOF), the PhenoGraph algorithm identified canonical CD45RO- (RO-) Tscm cells, as well as a Tscm-like subset that expressed CD45RO+ (RO+) (**Figure 1a**), which was confirmed using both CyTOF and flow biaxial gating strategies (**Figure 1b, Sup. Figure 1a, Sup. Figure 2a,b**). Cieri et al. recently described a RO+ Tscm cell subset in peripheral blood that could be generated from naïve T cells following IL-7 and IL-15 stimulation *in vitro*[12]. It is not known whether RO+ Tscm-like T cells originate from canonical (RO-) Tscm cells, or if this subset naturally exists in human cancer. We therefore tested the hypothesis that the RO+ Tscm-like TIL subset is a novel

downstream stem-like subset derived from canonical RO- Tscm cells. CD45RO+ Tscm-like TILs were present in human ovarian cancer at 1.07% ± 0.41% of overall CD3+ TILs, similar to canonical RO- Tscm TILs (0.92 ± 0.40%) (**Figure 1c**). The RO+ Tscm population was also detected in healthy PBL (3.93 ± 0.75%), ascites (1.74± 0.58%), and patient PBL (4.40± 1.70%) (**Sup. Figure 2a-c**). The RO- and RO+ Tscm TIL populations exhibited no significant differences in CD8+ T cell frequency (**Sup. Figure 2d**).

Similar expression patterns of CD27, CD28, CD11a and CD127 were observed between RO+ and RO- Tscm TIL subsets in tumor (**Figure 1d**). In healthy donor blood, the RO- Tscm and RO+ Tscm subsets also had similar frequency of CD27 expression, and both RO- and RO+ Tscm subsets from healthy PBL had a higher frequency of CD27 expressing cells than TILs (**Figure 1d,e**). While both RO- ($p < 0.001$) and RO+ Tscm TILs ($p < 0.001$) expressed greater levels of CXCR3, a chemokine receptor important for the infiltration of T cells into tumors[17], than naïve T cells, RO+ Tscm TILs expressed higher levels of CXCR3 than RO- Tscm TILs and other TIL subsets (**Figure 1d**). Given the relatively similar phenotypes of RO- and RO+ Tscm cells, we predicted that both subsets would similarly express TCF1, and confirmed this prediction using flow cytometry (**Figure 1f,g, Sup. Figure 2e,f)**.

We hypothesized that RO+ Tscm-like TILs are derived from the CD45RO- Tscm-like subset since CD45RO expression is characteristically indicative of more differentiated memory subsets[18]. To assess T cell differentiation patterning, sorted Naïve, RO- Tscm, RO+ Tscm, CM and EM T cells from ascites and healthy PBL were stained with CFSE and stimulated with IL-7 and IL-15 for 10 days, and proliferated (CFSE-diluted (**Sup. Figure 3a**)) cells analyzed by flow cytometry. RO- Tscm cells were found to exhibit self-renewal capability and multipotency, and, importantly, beget RO+ Tscm-like T cells whether they were derived from ascites (7.54 ± 3.91%)

or from healthy blood (28.23 ± 10.26%) (**Figure 2a-c**). RO+ Tscm cells from ascites (1 ± 0.39%) and from blood (4± 1.23%) were also capable of self-renewal and gave rise to CM, EM, and EFF T cells, but did not become CD45RO-, indicating that the RO+ Tscm cell subset is a distinct cell population downstream of canonical RO- Tscm T cells (**Figure 2a-c**). Similar results were also observed when TIL subsets were stimulated with autologous tumor cells (**Sup. Figure 3b,c**) or anti-CD3/CD28 activation beads (**Sup. Figure 3d**).

IL-7/15 cytokines are necessary for memory T cell maintenance[19] and are capable of generating Tscm cells from circulating naïve T cells[12], while IL-2 favors more terminal differentiation[20]. We therefore assessed if Tscm TIL subsets respond to these homeostatic cytokines. Healthy PBL derived RO- and RO+ Tscm cells both increased in frequency with IL-7/15 exposure, but not with IL-2 (**Figure 2d**). Similarly, the frequency of RO- Tscm TIL increased when cultured with IL-7/15 compared to IL-2. IL-7/15 exposure preserved RO+ Tscm TIL frequency while IL-2 exposure resulted in a decrease compared to media alone (p = 0.045) (**Figure 2e**), indicating that IL-7/15 exposure better maintains or promotes Tscm cells from both blood and tumor than IL-2. Since the mTOR pathway impacts T cell differentiation[21] and rapamycin can induce Tscm cell formation[22], we next investigated whether mTOR signaling contributes to Tscm cell maintenance by examining the impact of the mTORC1 inhibitor rapamycin on Tscm TIL subset frequency. There is an insignificant trend towards an increase in RO+ Tscm frequency following rapamycin treatment of PBL (p = 0.150, 0nM vs 200nM) and a significant increase in RO+ Tscm frequency following similar treatment of TILs (p = 0.042, 0nM vs 200nM). For both TILs from tumor and healthy PBLs, RO- Tscm cells tended to decrease in frequency following rapamycin treatment, although this was not significant (p = 0.149 for PBLs

p = 0.245 for TILs, 0nM vs 200nM) (**Sup. Figure 3e,f**). These results indicate that the two Tscm subsets differentially respond to mTORC1 inhibition.

Since RO+ Tscm cells are capable of differentiating into downstream memory subsets, we hypothesized that this subset of T cells would exhibit more T cell repertoire similarities (such as clonal expansion and overlap) with downstream memory subsets than with upstream RO- Tscm. Using three independent ovarian cancer ascites samples (1713, 1756, 1807), TCR sequencing was performed on sorted Naïve, RO- Tscm, RO+ Tscm, CM, EM, and EFF T cells. Each sorted subset had over 1000 clonotypes (see Methods Table 2 for immune repertoire profiling metadata). To evaluate the degree of clonal expansion in each of the T cell subsets, the proportion of high abundance clonotypes was analyzed using a rank plot, which revealed that both Tscm subsets had a level of clonal expansion that was higher than naïve but lower than EM or EFF T cell subsets (**Figure 3a**). As a second means of evaluating large clones, we analyzed their level of resampling within independently amplified and sequenced samples from each T cell subset. This analysis revealed that EM and EFF T cell populations had the highest proportions of resampled clones, as expected from their size distribution, while the RO+ Tscm TIL subset appeared to have an intermediate level of resampling, falling between RO- Tscm cells and CM T cells (**Figure 3b**). To gain insight into how clones traversed the different T cell subsets, we evaluated clonal overlap with the between-sample Jaccard index and found that RO+ Tscm T cell clones overlap more with downstream CM and EM memory subsets than with RO- Tscm T cell clones (**Figure 3c**). This is clear when viewing overlap between subsets for all productive rearrangements, where the RO+ Tscm T cell subset has greater overlap with both CM and EM subsets compared to the RO- Tscm subset (**Figure 3d**). Together with the in vitro assessments, these results support the notion that RO+ Tscm cells have a high degree of T cell

repertoire overlap with downstream memory subsets and may serve as a precursor pool for the generation of EM T cells which dominate the tumor microenvironment.

As our data supports the notion that RO+ Tscm cells give rise to and overlap with downstream memory subsets, we predicted that RO+ Tscm TILs would have greater expression of cytotoxic molecules compared to RO- Tscm cells. RO+ Tscm TILs exhibited enhanced expression of IFNγ ($p = 0.006$) and TNFα ($p= 0.028$) compared to RO- Tscm TILs and trended towards greater GranzymeB expression ($p = 0.107$) (**Figure 4a,b**). RO+ Tscm cells from healthy and patient blood expressed lower GranzymeB than EFF T cells, while RO+ Tscm cells from patient ascites had similar patterns of expression to RO+ Tscm TILs suggesting an influence by tumor cell exposure (**Sup. Figure 4a**). Notably, RO+ Tscm TILs were also identified in metastatic melanoma and colon tumors and expressed intermediate levels of GranzymeB compared to other memory subsets (**Sup. Figure 4b,c**).

To assess their relative effector function, RO- and RO+ Tscm cells were FACS sorted from three healthy PBLs and three ovarian ascites and stimulated with PMA/Ionomycin. The RO+ Tscm subset for all three healthy PBLs secreted more IFNγ than the RO- Tscm subset (**Figure 4c**). Tscm subsets from the three ovarian ascites samples followed a similar trend (**Figure 4d**), indicating that RO+ Tscm TILs are capable of exerting greater effector function than RO- Tscm. Interestingly, unstimulated RO+ Tscm TILs also express higher levels of CD137, a costimulatory receptor used to identify tumor-specific T cells[23,24], compared to RO- Tscm TILs ($p = 0.0165$) and CM ($p = 0.0222$) TILs (**Figure 4e**). CD137 expression by RO+ Tscm cells was highest in tumor (TILs), and low in peripheral blood T cells from both healthy and patient donors (**Sup. Figure 4d**). Taken together, these data suggest that RO+ Tscm TILs may be among

earliest tumor-infiltrating T cell memory subsets arising from RO- Tscm TILs capable of exerting anti-tumor functions.

RO+ Tscm TILs exhibit an effector profile but may experience inhibition in the tumor environment. In this line, RO+ Tscm TILs expressed greater levels of the inhibitory receptors PD-1 ($p < 0.001$), Lag-3 ($p < 0.001$), and TIGIT ($p = 0.043$), but equivalent expression of the activation marker CD69, compared to the RO- Tscm subset (**Figure 4f**). As expected, expression of PD-1, Lag-3, and TIGIT by RO+ Tscm TILs was higher in the tumor microenvironment, compared to blood (**Sup. Figure 4e**). Still, TCF-1+PD-1+ T cells mediate a proliferative response following checkpoint blockade and promote tumor control in mice[5], raising the possibility that human RO+ Tscm TILs co-expressing PD-1 and TCF1 may respond favorably to PD-1 blockade[5].

After performing RNAseq on Naïve, RO- Tscm, RO+ Tscm, CM, EM, and EFF T cells taken from three different patient tumor samples, we queried whether transcriptional differences distinguish the two Tscm subsets. The RO+ Tscm TIL subset harbored a unique transcriptional profile compared to Naïve, RO- Tscm, CM, EM, and EFF T cells (**Figure 5a**). The RO+ Tscm subset appeared transcriptionally intermediate between the RO- Tscm and CM subsets (**Figure 5b,c**). While there were a few differences in gene expression between Naïve and RO- Tscm TILs, RO+ Tscm TILs exhibited greater differences compared to Naïve cells, particularly in chemokine genes (*CXCL6, CXCL10, CXCL1*) and activation genes (*IL-6*, *FOXQ1*[25], *CD9*[26]) (**Figure 5b**). When comparing the two Tscm TIL subsets, RO- Tscm TILs had increased expression of *CCR7*, while RO+ Tscm TILs expressed greater levels of chemokine genes (*CXCL6*, *CXCL10, CXCL1, CXCL2, CCR8*) and genes involved in complement (*C1S, C2*) (**Figure 5b).** This was supported by gene ontology analysis, which revealed that, compared to

196 the RO- Tscm subset, RO+ Tscm TIL subsets expressed more genes involved in molecular
197 functions such as calcium ion binding, chemokine activity, and biological processes such as
198 chemokine-mediated signaling and complement activation (**Sup. Figure 5a**). Overall, these
199 gene signatures indicate that RO+ Tscm TILs express genes associated with active cell
200 migration and a pro-inflammatory role within the tumor environment.

201 RO+ Tscm TILs, compared to other differentiation subsets, show intermediate expression
202 of naivety associated genes such as *ACTN1, CD248, TAF4B, LEF1, TCF7,* and low expression
203 of *FOXP1* (**Figure 5c**). For effector associated genes, RO+ Tscm TILs exhibited intermediate
204 expression of (*PRDM1, HNRPLL, IFNG*), low expression of *B3GAT1*, and high expression of
205 *EOMES* and *TBX21* compared to other T cell differentiation subsets (**Figure 5c**). CM TILs
206 expressed higher levels of inhibitory/exhaustion related genes such as *PDCD1* (encoding PD-
207 1), *HAVCR2* (encoding Tim-3), *ENTPD1* (encoding CD39), *ICOS, CTLA-4,* and *TOX2*[27]
208 compared to RO+ Tscm TILs (**Figure 5b**). Interestingly, similar to RO- Tscm TILs, RO+ Tscm
209 TILs expressed lower relative levels of the aforementioned inhibitory/exhaustion genes, while
210 CM and EM subsets had high expression (**Figure 5c**). This suggests that the RO+ Tscm subset
211 may harbor early memory T cells that are not yet exhausted at the transcriptional level, given
212 that the RO+ Tscm TILs also express effector molecules, TCF1 and CD137 (**Figures 1f, 4a-e**).
213 Notably, functional early memory T cells appear necessary for immune checkpoint blockade
214 (ICB) efficacy, as a recent study by Caushi et al. found that patients with responses to ICB had
215 neoantigen-specific T cells exhibiting lower expression of exhaustion related genes and
216 increased expression of TCF1[28]. As such, our results may have implications in understanding
217 T cell exhaustion. For instance, Galletti et al. provided evidence that PD-1+TIGIT+ T cells are
218 committed to a dysfunctional lineage[29]. Although more research is needed, our data suggests

another possibility. Our finding that RO+ Tscm cells appear to be downstream of canonical Tscm T cells and express surface level PD-1 and TIGIT, but have low expression of inhibitory genes, suggests that an additional memory differentiation step occurs before T cells are committed to a dysfunctional lineage.

Given the importance of Tscm-like TILs for successful adoptive cell transfer (ACT)[14] and checkpoint blockade[3,5] therapies, we queried whether the gene expression profile of RO+ Tscm TIL is similar to that of previously described Tscm-like T cells associated with efficacious immunotherapy. We compared the gene expression profiles of the RO- and RO+ Tscm TILs to the stem-like T cell comparisons investigated by Krishna et. al. (CD39-CD69-)[14] and Im et al. (CXCR5+)[3]. The CD39-CD69- Tscm-like population vs CD39+CD69+ T cell subset gene expression comparison performed by Krishna et al. was similar to comparisons of RO+ Tscm vs EM (0.21) and to RO- Tscm vs CM (0.42) and EM (0.47) (**Figure 5d**). In addition, RO- and RO+ Tscm subsets had no differences in expression for CD39-CD69-, however the RO+ Tscm subset had a higher frequency of CD39+CD69+ TILs ($p = 0.033$) suggesting a more differentiated state (**Sup. Figure 5c**). Krishna et al. found that 3 out of 24 patients lacking CD39-CD69- TILs unexpectedly experienced a complete response to ACT[14]. Since some RO+ Tscm TILs express CD39+CD69+ and share features with the CD39-CD69- subset, it would be important to understand whether these 3 patients that responded to adoptive TIL therapy had RO+ Tscm TILs in their infusion product[14].

When comparing the Im et al. CXCR5+ subset analysis[3] with our data, both the RO- and RO+ Tscm subsets shared gene expression features to the CXCR5+ subset (**Sup. Figure 5b**). However, the RO+ Tscm TILs exhibited enhanced expression of CXCR5+Tim-3- ($p < 0.0001$) and no differences in Tim-3+CXCR5- compared to RO- Tscm TILs (**Sup. Figure 5c**), indicating

242 that, like CXCR5+ T cells, the RO+ Tscm subset may be highly responsive to PD-1 blockade.
243 Taken together, our results suggest that the RO- and RO+ Tscm subsets share similarities to
244 Tscm-like TILs in the literature that mediate successful ACT in melanoma patients[14] and
245 proliferate following PD-1 checkpoint blockade[3]. However, since the RO+ Tscm subset
246 expresses more CD137, effector molecules and secretes more proinflammatory cytokines than
247 the RO- Tscm subset, this novel memory precursor subset may be integral for the study of
248 natural anti-tumor responses and useful for investigator seeking to isolate and enrich early
249 memory tumor-specific T cells for adoptive TIL therapy[14,30].

250 Taken together, these findings have important implications for the fields of T cell
251 immunobiology and immunotherapy for ovarian cancer that may extend to other solid human
252 tumors. Our work shows that human ovarian tumors harbor a heterogenous population of Tscm-
253 like T cells that are capable of producing and maintaining the intratumoral TIL pool. Within the
254 Tscm TIL population, a novel CD45RO+ Tscm subset derived from canonical Tscm cells exists
255 that exhibits multipotency and effector characteristics. These cells have attributes indicative of
256 successful immunotherapy responses, and our findings lay the groundwork for investigating
257 agents and approaches to locally provoke RO+ Tscm cell activity in the tumor microenvironment
258 and improve immunotherapeutic efficacy against solid tumors.

Materials and methods

Tumor Samples. Viably frozen, human high-grade serous ovarian tumor or ascites samples were purchased from the Penn Ovarian Cancer Research Center (OCRC) Tumor BioTrust Collection. Ethics statement: All donor samples used in this study were de-identified and approved for use by the UPenn Institutional Review Board (IRB 702679, UPCC 17909). Sex and weight are not a biological variable as all tumor samples are from females. As samples are de-identified, age and weight are not known. Surgically resected tumors were procured from the operating room in an aseptic manner. Tissue was mechanically processed into fragments and added to an enzyme digest solution. A 10X stock solution of the enzyme digest buffer contains 2 mg/ mL collagenase (Sigma Aldrich) and 0.3kU/mL DNase I Type IV (Sigma Aldrich); solution was diluted to a 1x solution with RPMI 1640 at time of digestion. Tissue was incubated in the enzyme digest buffer overnight at room temperature on a rotator. Dissociated tumor tissue was subsequently filtered through sterile 100µm nylon mesh, centrifuged, and washed twice with dPBS (Dulbecco's Phosphate Buffered Saline). Ascites were centrifuged to isolate cells and washed twice in dPBS; cells were filtered through sterile 100 um nylon mesh between washes. Resultant tumor cell digests and ascites cells were cryopreserved in 10% dimethyl sulfoxide (DMSO) and human serum (Valley Biomedical, Inc., Product #HS1017). Samples were frozen at -80C and banked at -150C until further use.

Healthy donor peripheral blood T cells. Healthy donor peripheral blood mononuclear cells were purchased from the Human Immunology Core at the University of Pennsylvania.

Flow cytometry staining. Samples were centrifuged at 1300RPM and then washed once with PBS to remove DMSO. Samples were stained with live/dead aqua (ThermoFisher Cat# L34957) for 10 minutes to discriminate live and dead cells. Samples were washed twice with staining buffer (phosphate-buffered saline, 2% fetal bovine serum) to remove live/dead stain, then incubated at 4°C for 30 minutes in 50µl of an antibody cocktail to label human surface markers. Following staining, samples were washed three times before being run on a BD LSR Fortessa Flow Cytometer. For intracellular staining, after surface staining and washing, cells were fixed (BioLegend Fixation Buffer Cat# 420801) for 15 minutes at room temperature in the dark. Samples were centrifuged, supernatant discarded, then resuspended in 1x permeabilization wash buffer (BioLegend Cat# 421002) and centrifuged for 5minutes at 350g for a total of three times. Following the last centrifuge step, samples were resuspended in 50µl of intracellular antibody cocktail for 20min in the dark at room temperature. Following staining, samples were washed three times with 1x permeabilization wash buffer. Prior to acquisition on a Fortessa, samples were resuspended in staining buffer. The following anti-human antibodies were used: CD3 (PerCPCy5.5, BioLegend Cat# 317336, RRID:AB_2561628), CD8 (Pacific Blue, BioLegend Cat# 558207, RRID:AB_397058), CD45RA (APCCy7, BioLegend Cat# 304128, RRID:AB_10708880), CD45RO (BV570, BioLegend Cat# 304226, RRID:AB_2563818), CD45RO (FITC, BioLegend Cat# 304242, RRID:AB_2564159), CCR7 (PeCy7, BioLegend Cat# 353226, RRID:AB_11126145), CD95 (APC, BioLegend Cat # 305612, RRID:AB_314550), TCF1 (PE, Biolegend Cat# 655208, RRID:AB_2728492), CD39 (BV786, BD Biosciences Cat# 742523, RRID:AB_2740841), CD69 (BV650, BioLegend Cat# 310934, RRID:AB_2563158), CXCR5 (BV605, BD Biosciences Cat # 740379, RRID:AB_2740110), Tim-3 (BV711, BioLegend Cat # 345024, RRID:AB_2564046).

Mass Cytometry staining. All mass cytometry reagents were either bought from Fluidigm or conjugated in house using MAXPAR kits (Fluidigm). Antibody panel information is in Methods Table 1. Cell identifier stain Iridium191/193 (Cat# 201192A), identifier 127Idu (5-Iodo-2' -deoxyuridine, Cat# 201127), and Cisplatin 195 (Cat# 201195) were purchased from Fluidigm. All antibodies were titrated to determine optimal concentrations for staining samples. For downstream intracellular effector molecule detection, samples were treated with GolgiStop (BD Biosciences Cat# 554715, RRID:AB_2869009) 4-5 hours before staining. For staining, single-cell suspensions of donor samples were spun down, and incubated with 127IdU and cisplatin 195 in PBS for 10 minutes at room temperature to identify live/dead cells. Next, cells were washed in the MAXPAR cell staining buffer provided by Fluidigm (Cat #201068) and incubated for 30minutes at room temperature with an antibody cocktail containing all surface antibodies. Following surface marker incubation, cells were washed three times in staining buffer. To detect intracellular markers, cells were fixed for 30 minutes at room temperature in FOXP3 fixation/permeabilization working solution (eBioscience Cat# 00-5523-00), spun down, then 1x permeabilization buffer was added twice for 5minutes. Samples were incubated in intracellular antibody cocktail, made up in permeabilization buffer (permeabilization buffer from eBioscience Cat# 00-5523-00), for 2hrs. Samples were washed with three times with permeabilization buffer three times before being fixed in 1.6% PFA with 125nM Iridium 191/193 overnight at 4C. The next day, cells were washed 2x in PBS, then 1x in dH2O. Data acquisition was performed on a CyTOF Helios (Fluidigm) by the CyTOF Mass Cytometer Core at the University of Pennsylvania. The CyTOF core performed bead-based for all samples.

Methods Table 1

Antibodies	Source	Identifier	RRID
anti-human CD45 Clone HI30 89Y	Fluidigm	Cat # 3089003B	RRID:AB_2661851
anti-human CD11a Clone HI111 142Nd	Fluidigm	Cat # 3142006B	RRID:AB_2877095
anti- human CD4 Clone RPA-T4 143Nd	BioLegend	Cat # 300541	RRID:AB_2562809
anti-human CD69 Clone FN50 144Nd	Fluidigm	Cat # 3144018B	RRID:AB_2687849
anti-human CD8 Clone RPA-T8 146Nd	Fluidigm	Cat # 3146001B	RRID:AB_2687641
anti-human (cross) pStat5 Clone 47 147Sm	Fluidigm	Cat # 3147012A	RRID:AB_2661819
anti-human EOMES Clone 644730 148Nd	Novus Biologicals	Cat # MAB6166	N/A
anti-human Lag-3 Clone 11C3C65 150Nd	Fluidigm	Cat # 3150030B	N/A
anti-human CD107α Clone H4A3 151Eu	Fluidigm	Cat # 3151002B	N/A
anti-human TNFα Clone Mab11 152Sm	Fluidigm	Cat # 3152002B	N/A
anti-human Tim-3 Clone F382E2 153Eu	Fluidigm	Cat # 3153008B	RRID:AB_2687644
anti-human TIGIT Clone MBSA43 154Sm	Fluidigm	Cat # 3154016B	RRID:AB_2888926
anti-human PD-1 Clone EH12.2H7 155Gd	Fluidigm	Cat # 3155009B	RRID:AB_2687854
anti-human CXCR3 Clone G025H7 156Gd	Fluidigm	Cat # 3156004B	RRID:AB_2687646
anti-human (cross) pStat3 Clone 4/P-Stat3 158Gd	Fluidigm	Cat # 3158005A	RRID:AB_2661827
anti-human CCR7 Clone G043H7 159Tb	Fluidigm	Cat # 3159003A	RRID:AB_2714155
anti-human CD28 Clone CD28.2 160Gd	Fluidigm	Cat # 3160003B	RRID:AB_2868400
anti-human CTLA-4 Clone 14D3 161Dy	Fluidigm	Cat # 3161004B	RRID:AB_2687649
anti-human Ki67 Clone B56 162Dy	Fluidigm	Cat # 3162012B	RRID:AB_2888928
anti-human CD95 Clone DX2 164Dy	Fluidigm	Cat # 3164008B	RRID:AB_2858235

anti-human CD45RO Clone UCHL1 165Ho	Fluidigm	Cat # 3165011B	RRID:AB_2756423
anti-human IL-2 Clone MQ117H12 166Er	Fluidigm	Cat # 3166002B	N/A
anti-human CD27 Clone L128 167Er	Fluidigm	Cat # 3167006B	RRID:AB_2811093
anti-human IFNγ Clone B27 168Er	Fluidigm	Cat # 3168005B	N/A
anti-human CD45RA Clone HI100 169Tm	Fluidigm	Cat # 3169008B	N/A
anti-human CD3 Clone UCHT1 170Er	Fluidigm	Cat # 3170001B	RRID:AB_2811085
anti-human Granzyme B Clone GB11 171Yb	Fluidigm	Cat # 3171002B	RRID:AB_2687652
anti-human CD57 Clone HCD57 172Yb	Fluidigm	Cat # 3172009B	RRID:AB_2888930
anti-human CD137 Clone 4B4-1 173Yb	Fluidigm	Cat # 3173015B	N/A
anti-human HLA-DR Clone L243 174Yb	Fluidigm	Cat # 3174001B	RRID:AB_2665397
anti-human Perforin Clone BD48 175Yb	Fluidigm	Cat # 3175004B	N/A
anti-human CD127 Clone A019D5 176Yb	Fluidigm	Cat # 3176004B	RRID:AB_2687863

Mass cytometry biaxial analyses. Traditional biaxial analysis, on bead-normalized fcs files, was performed using Flowjo V10 software (FlowJo, RRID:SCR_008520). Intact single cells were identified using event-length and Iridium. Cells were live-gated according to 127IdU and cisplatin 195, where dead cells are positive for cisplatin 195. CD3 and CD45 positivity identified T-cells. Sequential gating analysis was performed for all analyzed markers. The resulting values were used to determine population frequencies.

PhenoGraph analysis. High-dimensional analysis was conducted using the algorithm PhenoGraph from *cyt* a visualization tool written in Matlab (R2016b,

MATLAB,RRID:SCR_001622) downloaded in 2015 and available at https://www.c2b2.columbia.edu/danapeerlab/html/cyt-download.html. Live, single, $CD3^+CD45^+$ exported fcs data from five donor samples were imported into *cyt*, arcsinh5-transformed, with 8100 events randomly subsampled from each donor. The PhenoGraph algorithm was run, as described by Levin et al., 2015[31], with a nearest neighbor input of k=30 and a Euclidean distance metric. Markers used for PhenoGraph clustering were the following: CD95, CD27, CXCR3, CD28, CD45RO, CD11a, CCR7, CD45RA, CD57, CD127. PhenoGraph plots were created by *cyt*.

Fluorescent-Activated Cell Sorting. Tumor samples were thawed and washed twice with staining buffer to remove DMSO. Samples were subsequently stained with live/dead aqua for 10 minutes to discriminate live and dead cells. Samples were washed twice to remove live/dead aqua, then incubated at 4°C for 30 minutes in 50ul of an antibody cocktail to label human surface markers. Following surface staining, samples were washed three times with staining buffer. Samples were sent to the Flow Cytometry Core at the Children's Hospital of Philadelphia or sent to the Penn Cytomics and Cell Sorting Resource Laboratory and sorted on a FACSAria Fusion. All antibodies were purchased from BioLegend. For all analyses, singlets were detected, then cells negative for live/dead aqua, were identified as live cells. Experiments sorting overall Tscm T cells used the following anti-human antibodies: CD3 (APCCy7, Cat# 300318, RRID:AB_314054) to detect T cells, followed by CD45RA (Pacific Blue, Cat# 304118, RRID:AB_493657), CCR7 (PeCy7, Cat# 353226, RRID:AB_11126145), and CD95 (APC, Cat # 305612, RRID:AB_314550) to identify T cell differentiation subsets. For experiments delineating Tscm RO- and Tscm RO+ T cells (including RNA and TCR sequencing experiments), anti-

human-CD3 (BV605, Cat# 317322, RRID:AB_2561911) was used to detect T cells and the following anti-human antibodies were used to identify T cell differentiation subsets: CD45RA (APCCy7, Cat# 304128, RRID:AB_10708880), CD45RO (FITC, Cat# 304242, RRID:AB_2564159), CCR7 (PeCy7, Cat# 353226, RRID:AB_11126145), CD95 (APC, Cat # 305612, RRID:AB_314550). The experiment testing RO- and RO+ Tscm T cells response to PMA/Ionomycin stimulation using the Cell Stimulation Cocktail (500x) (eBioscience, Cat# 00-4970-03) used the following antibodies to sort: CD3 (PerCPCy5.5, BioLegend Cat# 317336, RRID:AB_2561628) for T cell identification, then CD45RA (APCCy7, Cat# 304128, RRID:AB_10708880), CD45RO (BV570, BioLegend Cat# 304226, RRID:AB_2563818), CCR7 (PeCy7, Cat# 353226, RRID:AB_11126145), CD95 (APC, Cat # 305612, RRID:AB_314550) to identify T cell differentiation subsets.

Differentiation and multipotency experiments. Naïve, Tscm (CD45RO- and CD45RO+), Tscm CD45RO-, Tscm CD45RO+, CM, and EM subsets were sorted as described above. Following sorting, subsets were stained with 10 μM CFSE (ThermoFisher Cat# C34554) for 10 minutes at 37C, washed twice with staining buffer, then plated at equal numbers per well in a 96 u-bottom plate. For the differentiation experiment testing Tscm-like T cells without discriminating for CD45RO expression, samples were subsequently stimulated with CD3/CD28 beads at a 0.3:1 bead to T cell ratio. Cells were fed 100ng/ml IL-7 and IL-15 every other day. On day 7 samples were de-beaded and on day 14 samples were analyzed on a Fortessa. For the differentiation experiment analyzing CD45RO- and CD45RO+ Tscm-like T cells subsets, following sorting and CFSE staining, cells were either provided 100ng/ml IL-7 and IL-15 every other day only, or were stimulated with TransAct (Miltenyi Biotec, Cat# 130-111-160) at a 1:1

CD3/CD28 to cell ratio and provided 100ng/ml IL-7/IL-15 every other day, then analyzed on day 10 on a Fortessa.

Cytokine experiment. Ovarian patient tumor digest cell suspensions were thawed, washed twice in media to remove DMSO, then rested overnight without cytokine at a concentration of 2million/ml. The following day, cells were plated in 96u-bottom plate at 300,000 cells per well and treated for the following conditions: no cytokine (PBS added), 50IU/ml IL-2, or 50ng/ml IL-7 and 50ng/ml IL-15. Samples were stained and analyzed the following day for T cell differentiation phenotype via flow.

Rapamycin, mTOR inhibitor, experiment. Ovarian patient tumor digest cell suspensions were thawed, washed twice in media to remove DMSO, then rested overnight without cytokine at a concentration of 2million/ml. The following day, cells were plated in 96u-bottom plate at 400,000 cells per well and treated for the following conditions: untreated (DMSO added), 50nM, 100nM, or 200nM rapamycin. Samples were stained and analyzed the following day for T cell differentiation phenotype via flow.

RO- and RO+ Tscm T cell stimulation experiment. Healthy donor PBMCs and ovarian patient ascites were FACS sorted for RO- and RO+ Tscm T cells as described in the Fluorescent-Activated Cell Sorting section of the methods. RO- and RO+ Tscm T cells were plated in equal cell numbers in a 96 u-bottom well plate per each donor, for a resting and stimulated condition. Healthy donor 543 had 28,000 RO- and RO+ Tscm T cells plated per well in triplicates in 130ul media (RPMI 1640 media supplemented with 10% fetal bovine serum) per well. Healthy donor

567 had 10,000 RO- and RO+ Tscm T cells plated per well in triplicates in 130ul media per well. Healthy donor 570 had 7,500 RO- and RO+ Tscm T cells plated per well in triplicates in 130ul media per well. Patient ascites 1793 had 320 RO- and RO+ Tscm T cells plated per well with in 65ul media due to low cell number obtained. For the stimulated condition, T cells were provided 1x of the Cell Stimulation Cocktail (500x) (eBioscience, Cat# 00-4970-03) for 24hrs. The following day, samples were spun at 1300RPM and 110ul of supernatant was removed for each healthy donor sample and 50ul was removed for the ascites sample. Supernatants were frozen at -80C. To analyze IFNg within the supernatants, the LEGENDplex Human CD8/NK Panel kit (BioLegend, Cat# 740267) was used following the manufacturer's protocol.

TCRβ sequencing. Ovarian ascites samples from three human donors (1713, 1756, and 1807) were sorted by flow cytometry to isolate bulk CD3+ T cells and were further sorted to differentiate six subsets: Naïve (CD45RA+CCR7+CD95-CD45RO-), RO- (Tscm (CD45RA+CCR7+CD95+CD45RO-), RO+ Tscm (CD45RA+CCR7+CD95+CD45RO+), CM (CCR7+CD45RA-), EM (CCR7-CD45RA-), and EFF (CCR7-CD45RA+) T cells. Additionally, CD3+ tumor-infiltrating lymphocytes were sorted from patient matched tumor digest samples. Refer to the Fluorescent-Activated Cell Sorting section of the methods for information regarding specific antibodies used.

DNA was extracted from sorted T cells using a Gentra Puregene Cell kit (Catalog # 158767, Qiagen). T cell receptor beta chain (TCRβ) rearrangements were amplified using the immunoSEQ Assay (Catalog # ISK10050, Adaptive Biotechnologies, Seattle, WA) in the Human Immunology Core Facility at the University of Pennsylvania and were sequenced with an Illumina

NextSeq 500/550 Mid Output Kit v2.5 (150 Cycles) (Catalog # 20024904). The input DNA was normalized for all samples with few exceptions (Methods Table 2).

TCRβ data analysis. Sequencing data were exported from the Adaptive Biotechnologies website for downstream analysis. Only productive rearrangements from the Adaptive's sample sheet were used in all the analyses. The metadata table (Methods Table 2) shows the summary of the total copies (templates) of all productive rearrangements and the total number of unique productive rearrangements as defined by Adaptive Biotechnologies.

Methods Table 2. TCRβ Sequencing Metadata

sample ID	DNA input (ng) per replicate	# replicates	total templates for productive rearrangements	productive rearrangements
1713-ascites-CM	50	2	31638	16496
1713-ascites-EFF	50	2	28054	2444
1713-ascites-EM	50	2	25519	4819
1713-ascites-Naive	50	2	13864	9588
1713-ascites-TscmROneg	50	2	41757	26913
1713-ascites-TscmROpos	50	2	33501	14509
1756-ascites-CM	50	2	29425	13892
1756-ascites-EFF	45.8	2	26929	2548
1756-ascites-EM	20.4	2	11869	2867
1756-ascites-Naive	50	2	30012	23218
1756-ascites-TscmROneg	31	2	20616	9334
1756-ascites-TscmROpos	50	2	24533	10984
1807-ascites-CM	50	2	36465	17292
1807-ascites-EFF	50	2	35182	7951
1807-ascites-EM	50	2	48310	9836
1807-ascites-Naive	50	2	26244	17227
1807-ascites-TscmROneg	50	2	46144	28291
1807-ascites-TscmROpos	50	2	49922	21265

Bulk RNA sequencing and analysis. FACS sorting was performed on one reference healthy donor PBMC sample and three different human ovarian tumor samples to isolate the following

T cell differentiation subsets: Naïve, RO- Tscm, RO+ Tscm, CM, EM, and EFF T cells. Bulk RNA sequencing of all sample subsets was performed by the University of Pennsylvania Next-Gen Sequencing Core (NGSC). Jonathan Schug and previous NGSC core member Shilpa Rao created the heatmap, volcano plots, gene transcription trends, and performed gene ontology analysis. Total RNA was extracted from roughly 500 cells per sample (T cell differentiation subset) using the GenElute SingleCell kit (Sigma-Aldrich, Cat# RNB300). The resulting RNA was converted to cDNA and amplified using the SMARTer Universal Low Input RNA kit for sequencing (Clontech/Takara, Cat# 634940). This cDNA was then converted to Illumina RNA-Seq libraries using the Illlumina Nextera library prep kit (Illumina, Cat# FC-131) with median length of 622 +/- 51bp and molarity of 11.8 +/1 4.3 nM as measured on the Agilent BioAnalyzer. Libraries were sequenced on an Illumina HiSeq 4000 to a depth of 20.4 MR +/- 5.2 using 100bp single-end reads. The reads were adapter trimmed, filtered for quality, then aligned to the human genome (hg19) using the RUM program which also quantifies expression[32]. Using the RefSeq transcript expression quantification, differentially expressed genes were identified using edgeR[33,34] using a design that took the donor ID into consideration.

John Tobias of the Molecular Profiling Facility, Bioinformatics (Penn) analyzed differential gene comparison between our data and data in the literature, specifically CD39-CD69- vs CD39+CD69+[14] T cell subsets and CXCR5+Tim-3- vs CXCR5-Tim-3+[3] T cell subsets. Log2FC for contrasts of interest were merged and subsequently merged with log2FC changes for the genes filtered for significance from each of the datasets. For the CD39-CD69- vs CD39+CD69+ comparison, differential expression values from the supplement were filtered with cutoffs for 2-fold up or down and an FDR-adjusted p-value of <0.1, which left 992 significant genes also present in our data. For CXCR5+ vs Tim-3+ comparison, the contrast was calculated in

Transcriptome Analysis Console (v4, Thermo Fisher). Raw data (CEL files) were normalized using RMA, and the contrast was calculated and filtered for at least 2-fold up or down and an FDR-adjusted p-value of < 0.01. This left 1447 significant genes also present in our data.

Statistical analysis. All statistical parameters are described in figure legends. Student's *t*-tests (two-tailed, paired, or two-tailed, unpaired) or one-way ANOVA (paired) were performed using GraphPad Prism v.9 (GraphPad Software) to determine statistical significance. Data was assumed to have normal distribution for all statistical tests. NS represents a p-value >0.050, (*) represents a p-value ≤0.050, (**) represents a p-value <0.01, (***) represents a p-value < 0.001, (****) represents a p-value < 0.0001, error bars represent the standard error of the mean (SEM). In the box and whisker plots the box represents the median and upper and lower quartiles and the whiskers the minimum and maximum values.

Code availability. RNAseq data analysis was completed by the University of Pennsylvania NGSC and the Molecular Profiling Facility, Bioinformatics (Penn). Code is available upon reasonable request.

Data availability. RNAseq raw and processed data is publicly available on the gene expression omnibus (GEO), under accession number GSE188209. TCRβ data will be shared on the immuneACCESS database hosted by Adaptive Biotechnologies. Reviewers can access data before it is publicly available at https://clients.adaptivebiotech.com/login using the login email eiva-review@adaptivebiotech.com and password "eiva2021review".

References

1. Morrot, A. Human stem memory T cells (TSCM) as critical players in the long-term persistence of immune responses. *Ann. Transl. Med.* **5**, (2017).
2. Cieri, N. *et al.* Generation of human memory stem T cells after haploidentical T-replete hematopoietic stem cell transplantation. **125**, 2865–74 (2015).
3. Im, S., Hashimoto, M., Gerner, M., Lee, J. & Kissick, H. Defining CD8+ T cells that provide the proliferative burst after PD-1 therapy. (2016).
4. Gattinoni, L. Memory T cells officially join the stem cell club. *Immunity* **41**, 7–9 (2014).
5. Siddiqui, I. *et al.* Intratumoral Tcf1+PD-1+CD8+ T Cells with Stem-like Properties Promote Tumor Control in Response to Vaccination and Checkpoint Blockade Immunotherapy. *Immunity* **50**, 195-211.e10 (2019).
6. Gattinoni, L. *et al.* A human memory T cell subset with stem cell-like properties. *Nat Med* **17**, 1290–7 (2011).
7. Biasco, L. *et al.* Clonal expansion of T memory stem cells determines early anti-leukemic responses and long-term CAR T cell persistence in patients. *Nat. Cancer* **2**, 629–642 (2021).
8. Biasco, L. *et al.* In vivo tracking of T cells in humans unveils decade-long survival and activity of genetically modified T memory stem cells. **7**, 273ra13 (2015).
9. Mpande, C. A. M. *et al.* Functional, Antigen-Specific Stem Cell Memory (TSCM) CD4+ T Cells Are Induced by Human Mycobacterium tuberculosis Infection. *Front. Immunol.* **9**, (2018).
10. Liu, Q., Sun, Z. & Chen, L. Memory T cells: strategies for optimizing tumor immunotherapy. *Protein Cell* **11**, 549–564 (2020).

11. Gattinoni, L., Speiser, D. E., Lichterfeld, M. & Bonini, C. T memory stem cells in health and disease. *Nat Med* **23**, 18–27 (2017).
12. Cieri, N. *et al.* IL-7 and IL-15 instruct the generation of human memory stem T cells from naive precursors. *Blood* **121**, 573–584 (2013).
13. Galletti, G. *et al.* Two subsets of stem-like CD8 + memory T cell progenitors with distinct fate commitments in humans. *Nat. Immunol.* **21**, 1552–1562 (2020).
14. Krishna, S. *et al.* Stem-like CD8 T cells mediate response of adoptive cell immunotherapy against human cancer. *Science* **370**, 1328–1334 (2020).
15. Jansen, C. S. *et al.* An intra-tumoral niche maintains and differentiates stem-like CD8 T cells. *Nature* **576**, 465–470 (2019).
16. Zhao, X., Shan, Q. & Xue, H.-H. TCF1 in T cell immunity: a broadened frontier. *Nat. Rev. Immunol.* 1–11 (2021) doi:10.1038/s41577-021-00563-6.
17. Dangaj, D. *et al.* Cooperation between Constitutive and Inducible Chemokines Enables T Cell Engraftment and Immune Attack in Solid Tumors. *Cancer Cell* **35**, 885-900.e10 (2019).
18. Gattinoni, L., Speiser, D. E., Lichterfeld, M. & Bonini, C. T memory stem cells in health and disease. *Nat. Med.* **23**, 18–27 (2017).
19. Abdelsamed, H. A., Zebley, C. C. & Youngblood, B. Epigenetic Maintenance of Acquired Gene Expression Programs during Memory CD8 T Cell Homeostasis. *Front. Immunol.* **9**, (2018).
20. Ross, S. H. & Cantrell, D. A. Signaling and Function of Interleukin-2 in T Lymphocytes. *Annu. Rev. Immunol.* **36**, 411–433 (2018).
21. Waickman, A. T. & Powell, J. D. mTOR, metabolism, and the regulation of T-cell differentiation and function. *Immunol. Rev.* **249**, 43–58 (2012).

22. Scholz, G. *et al.* Modulation of mTOR Signalling Triggers the Formation of Stem Cell-like Memory T Cells. *EBioMedicine* **4**, 50–61 (2016).
23. Ye, Q. *et al.* CD137 accurately identifies and enriches for naturally occurring tumor-reactive T cells in tumor. *Clin Cancer Res* **20**, 44–55 (2014).
24. Parkhurst, M. *et al.* Isolation of T-Cell Receptors Specifically Reactive with Mutated Tumor-Associated Antigens from Tumor-Infiltrating Lymphocytes Based on CD137 Expression. *Clin Cancer Res* **23**, 2491–2505 (2017).
25. Bupp, M. R. G. & Peng, S. L. The forkhead transcription factor Foxq1 enhances NF-kB activity and is critical for robust T cell activation and autoimmunity (35.22). *J. Immunol.* **178**, S5–S6 (2007).
26. Kobayashi, H. *et al.* The tetraspanin CD9 is preferentially expressed on the human CD4(+)CD45RA+ naive T cell population and is involved in T cell activation. *Clin. Exp. Immunol.* **137**, 101–108 (2004).
27. Seo, H. *et al.* TOX and TOX2 transcription factors cooperate with NR4A transcription factors to impose CD8+ T cell exhaustion. *Proc. Natl. Acad. Sci.* **116**, 12410–12415 (2019).
28. Caushi, J. X. *et al.* Transcriptional programs of neoantigen-specific TIL in anti-PD-1-treated lung cancers. *Nature* 1–7 (2021) doi:10.1038/s41586-021-03752-4.
29. Galletti, G. *et al.* Two subsets of stem-like CD8+ memory T cell progenitors with distinct fate commitments in humans. *Nat. Immunol.* **21**, 1552–1562 (2020).
30. Vanmeerbeek, I. *et al.* Early memory differentiation and cell death resistance in T cells predicts melanoma response to sequential anti-CTLA4 and anti-PD1 immunotherapy. *Genes Immun.* **22**, 108–119 (2021).

31. Levine, J., Simonds, E., Bendall, S. & Davis, K. Data-driven phenotypic dissection of AML reveals progenitor-like cells that correlate with prognosis. (2015).
32. Grant, G. R. *et al.* Comparative analysis of RNA-Seq alignment algorithms and the RNA-Seq unified mapper (RUM). *Bioinforma. Oxf. Engl.* **27**, 2518–2528 (2011).
33. McCarthy, D. J., Chen, Y. & Smyth, G. K. Differential expression analysis of multifactor RNA-Seq experiments with respect to biological variation. *Nucleic Acids Res.* **40**, 4288–4297 (2012).
34. Robinson, M. D., McCarthy, D. J. & Smyth, G. K. edgeR: a Bioconductor package for differential expression analysis of digital gene expression data. *Bioinforma. Oxf. Engl.* **26**, 139–140 (2010).

Acknowledgements. The authors acknowledge the Ovarian Cancer Translational Center for Excellence in the Abramson Cancer Center for support of tumor banking operations through the Tumor BioTrust Collection, in particular Dalia K. Omran and Euihye Jung. The authors also thank Dr. Bertram Bengsch, previous member of the E. John Wherry laboratory at the University of Pennsylvania (UPenn), for CyTOF training, and Takuya Ohtani of the UPenn CyTOF Core for running mass cytometry samples. The authors also acknowledge support from the Flow Cytometry Core Laboratory at the Children's Hospital of Philadelphia Research Institute, the Penn Cytomics and Cell Sorting Resource Laboratory, and the Flow Cytometry Facility at the Wistar Institute. The authors thank Jonathan Schug, Shilpa Rao and Olga Smirnova of the UPenn Next-Gen Sequencing Core (NGSC) and John Tobias of the UPenn Molecular Profiling Facility for their aid in RNAseq experimentation and bioinformatics analysis.

Author contributions. Conceptualization, methodology, writing-original draft, writing-review & editing, visualization, M.A.E. and D.J.P. Resources, supervision, funding acquisition, D.J.P. Validation, investigation, formal analysis, M.A.E. Validation, investigation, formal analysis, writing-review & editing, E.G.B. Validation, investigation, writing-review & editing, V.P., A.B.B. Validation, investigation, S.T. Formal analysis, investigation, validation, writing-review & editing, visualization, W.M., A.R., E.L.P.

Competing Interests.

D.J.P. holds a patent on CD137 enrichment for efficient tumor infiltrating lymphocyte selection (U.S. Pat. No. 10,233,425) and receives fees for advisory services from InsTIL Bio on TIL therapy. All other authors have no commercial or financial conflicts of interests.

Funding.

This work was supported in part by a pilot grant from NCI/NIH SPORE P50 CA228991 awarded to Daniel J. Powell Jr., and partly by NCI/NIH R01-EB-026892, a gift from the Kronish Research Foundation for the Treatment of Ovarian Cancer and by BMS grant CA186-113 awarded to Jessica A. Chacon and Daniel J. Powell Jr. The funding sources had no role in the design, collection, analysis, interpretation, writing, or decision to submit the manuscript for publication.

Figures

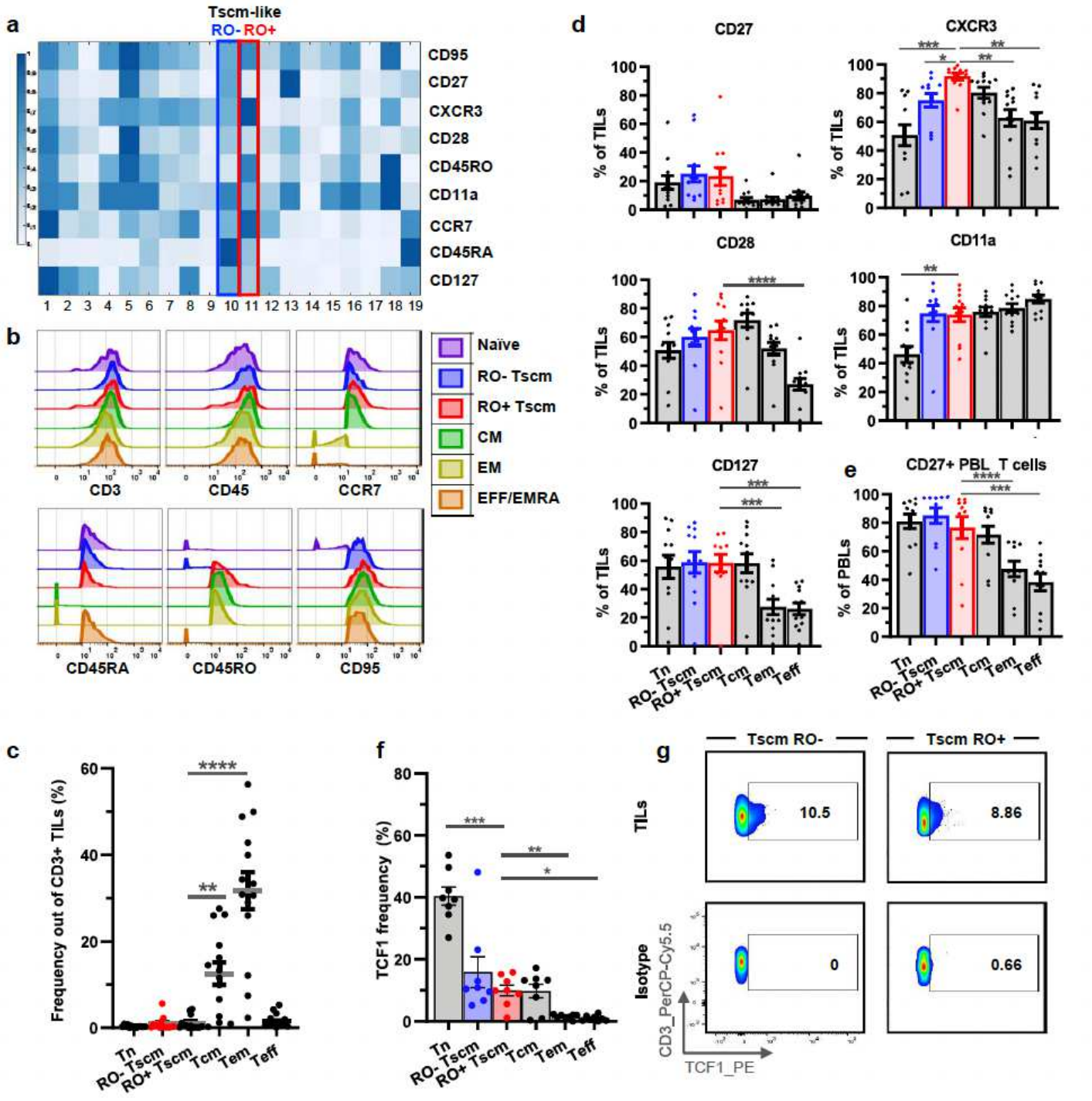

Figure 1

Interrogation of Tscm-like TIL heterogeneity in solid human tumors reveals a Tscm-like T cell expressing CD45RO. (a) PhenoGraph clustering heatmap representative of 5 different ovarian cancer patient TILs interrogated by CyTOF. (b) Histograms showing expression of different memory markers for each TIL differentiation subset from representative patient TILs analyzed by CyTOF. (c) Frequency of each TIL

differentiation subset out of overall live CD3+CD45+ TILs (n=14). (d) Expression of different memory markers within each TIL differentiation subset, CyTOF analysis (n=12). (e) Expression of CD27 within each T cell differentiation subset for healthy PBL T cells, CyTOF analysis (n=11). (f) Expression of TCF1 within each TIL differentiation subset, flow analysis (n=8). (g) Representative flow gating for TCF1 expression analysis for RO- and RO+ Tscm TIL subsets, isotype example included. One-way ANOVA, Tukey's multiple comparisons test. Only significant differences compared to the Tscm RO+ group are marked. (*) represents a p-value 0.050, (**) represents a p-value <0.01, (***) represents a p-value <0.001, (****) represents a p-value < 0.0001, error bars represent the standard error of the mean (SEM). All experiments were independently performed at least twice.

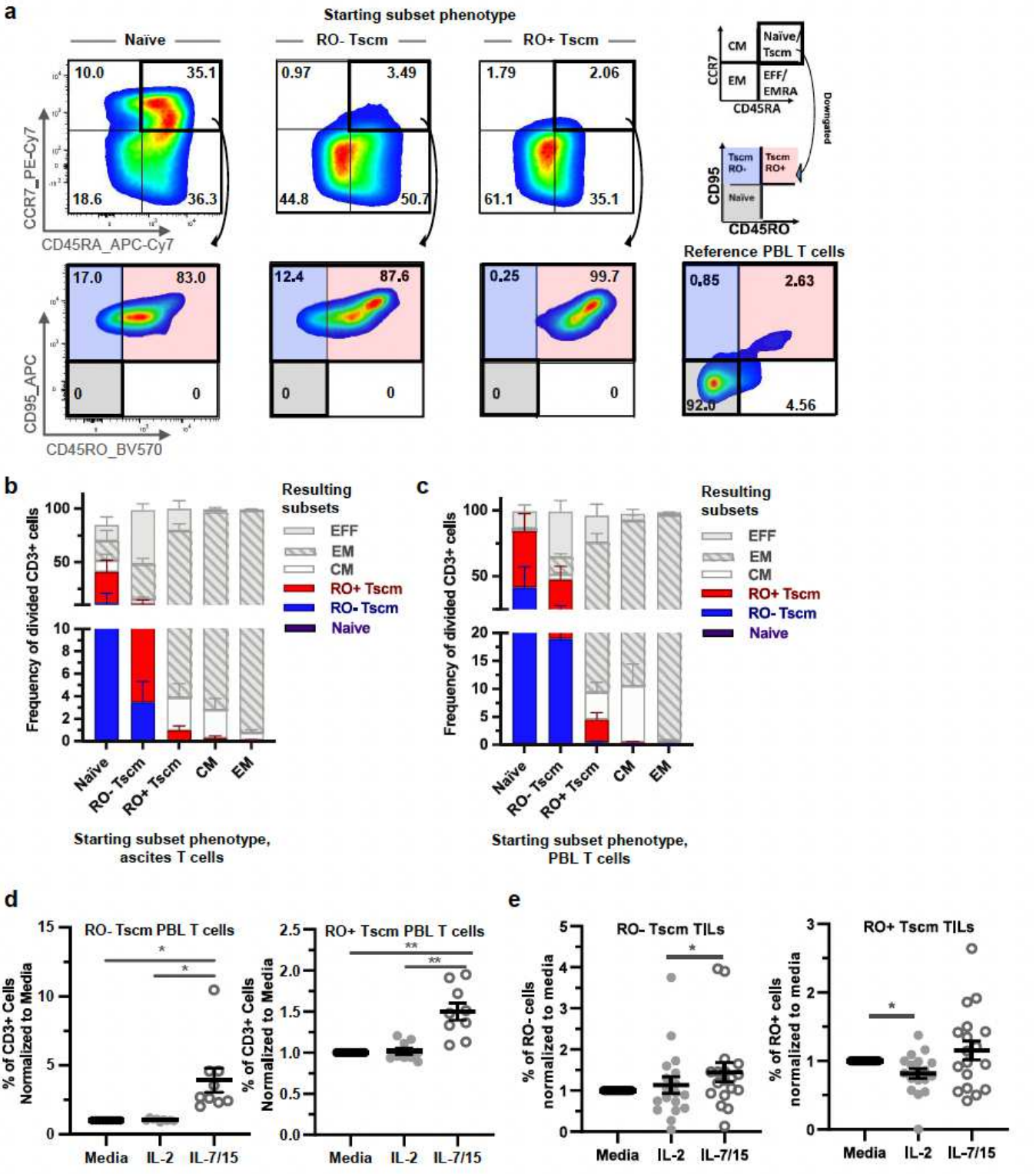

Figure 2

CD45RO+ Tscm T cells self-renew, are multipotent, and are derived from canonical CD45RO- Tscm T cells. (a) Representative gating phenotype of proliferated T cells that began as na ve (first column), RO- Tscm (second column), and RO+ Tscm (third column) T cells from patient ascites. T cells were stimulated with 100ng/ml IL-7/IL-15 every other day and analyzed via flow on day 10. Gating schema is on the upper right, and representative PBL T cells the CD45RO vs CD95 gate is on the bottom right. (b) Bar plots

representing what each starting T cell differentiation subset became following cytokine stimulation. Samples were phenotyped on day 10 and represent the phenotype of proliferated (CFSE diluted) cells (n=4 ascites T cells). (c) Same as b, but starting material was PBL T cells from healthy donor peripheral blood (n=3). (d) PBL T cells treated with either no cytokine (media), 50IU/ml IL-2, or 50ng/ml IL-7 and 50ng/ml IL-15 for 24hrs, and phenotyped via flow. Plots represent frequency of RO- and RO+ Tscm TILs normalized to the media alone condition (n=9). (e) Same experiment as in d, however starting material is Tumor digests (n=18). One-way ANOVA, Tukey's multiple comparisons test. (*) represents a p-value 0.050, (**) represents a p-value <0.01, (***) represents a p-value < 0.001, error bars represent the standard error of the mean (SEM). All experiments were independently performed at least twice.

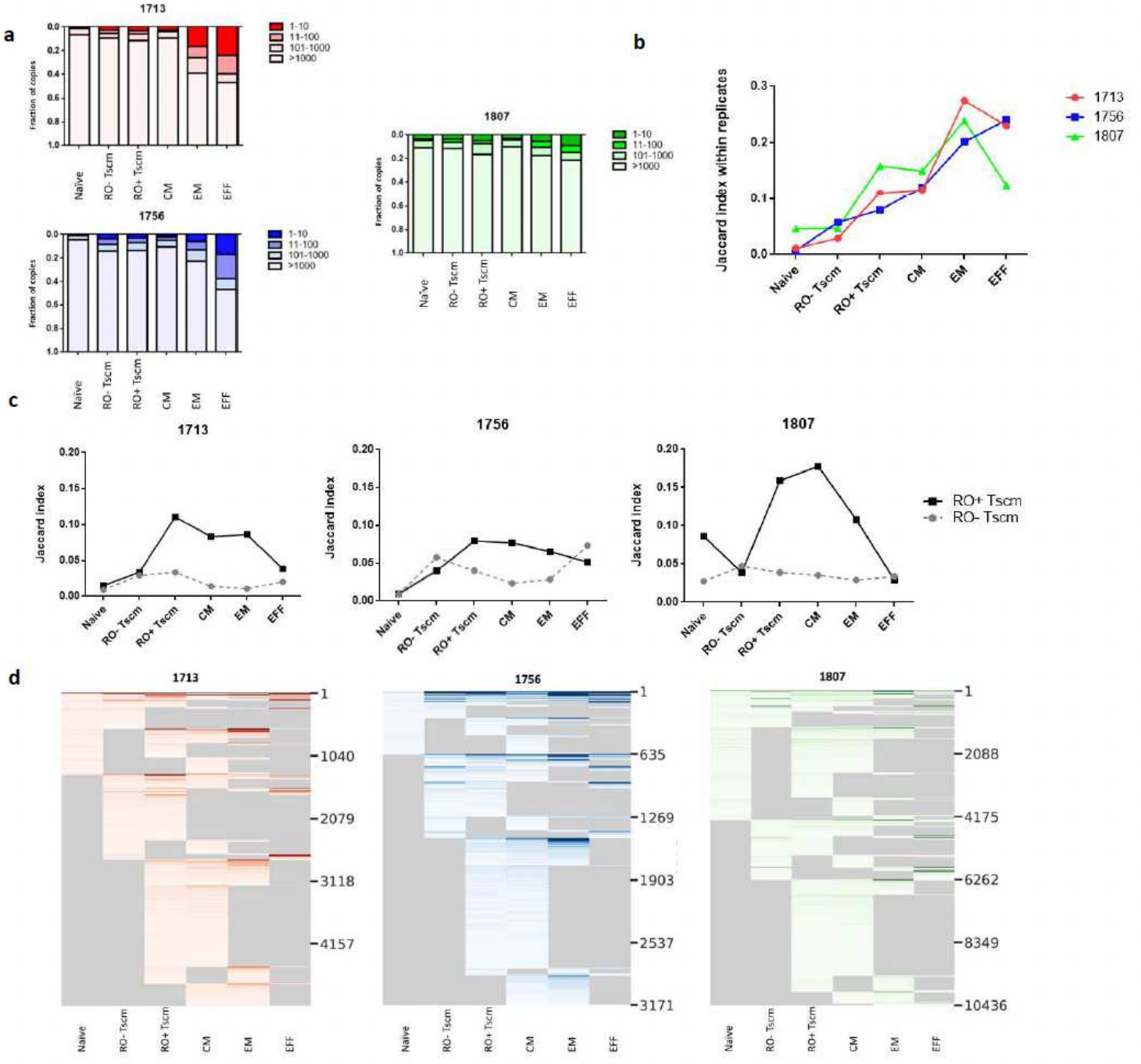

Figure 3

TCRβ gene rearrangement analysis in T-cell subsets, CD45RO+ Tscm T cell repertoire overlaps with downstream memory subsets. TCRβ sequencing was performed on FACS sorted cells across 6 subsets: na ve, CD45RO- Tscm, CD45RO+ Tscm, CM, EM, and EFF T. (a) Range plots on rearrangements size distribution. The fraction of sequence copies that comprise productive rearrangements of different size categories in each of the three donors. The EM and EFF populations have the largest rearrangements compared to the other subsets. (b) The Jaccard index was computed between independently amplified sequencing libraries from each replicate. To compare the subsets within each donor, measures were connected (even though they are discrete and unrelated) and curves were colored by individual patient. Consistent with the rank plot, EM and EFF populations had the highest proportions of resampled clones. (c) Between-sample Jaccard Index. Jaccard index was computed on overlapping rearrangements in RO- Tcsm (dash line) and RO+ Tcsm (solid line) subsets with other subsets and plotted for each patient. RO+ Tcsm had more overlap with the CM and EM than RO- Tcsm subset. (d) Overlapping rearrangements across subsets. Each row is a productive rearrangement, each column is a cell subset, and the intensity of each combination represents the copy number fraction of the given rearrangement in the given subset where darker colors indicate higher copy number fraction. Grey means no data. Only rearrangements in at least two subsets were included in the plot. Numbers of overlapping rearrangements are shown to the right of each plot.

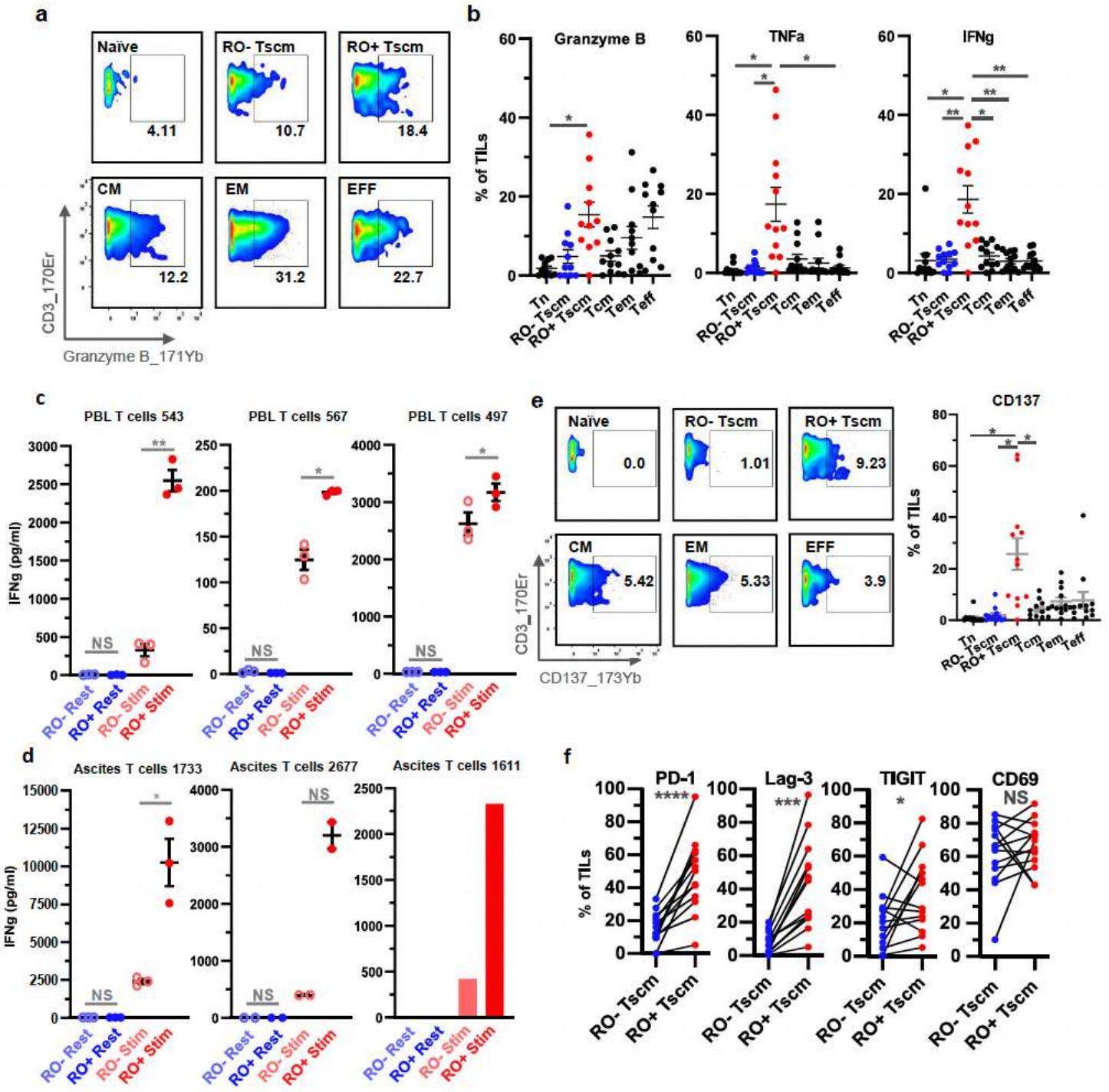

Figure 4

The CD45RO+ Tscm TIL subset exhibits an effector profile indicative of tumor-specificity. (a) Example CyTOF gating for Granzyme B expression within TIL differentiation subsets. (b) Expression of Granzyme B, IFNγ, IFNα within each TIL differentiation subset (n=14 Tcm, Tem, Teff, n= 13 RO-Tscm RO+ Tscm, n=11 Tn). (c-d) FACS sorted RO- and RO+ T cells obtained from three different healthy donor peripheral blood mononuclear cells (c) or three patient ovarian ascites (d) were either stimulated with 1x of Cell Stimulation Cocktail for 24hrs or allowed to rest, and 24hr supernatants were analyzed for IFNg secretion

(points indicate replicates from each sample). (e) (Left) CyTOF gating for CD137 expression within TIL differentiation subsets. (Right) CD137 expression within TIL differentiation subsets (n=12). (f) Expression of PD-1, Lag-3, TIGIT, and CD69 within RO- and RO+ Tscm TILs (n=13). Student's two-tailed, paired t-test was used for c, d and f. One-way ANOVA, Tukey's multiple comparisons test was used for b, e. Only significant differences compared to the Tscm RO+ group are marked for multiple comparisons. NS represents a p-value >0.050, (*) represents a p-value 0.050, (**) represents a p-value <0.01, (***) represents a p-value < 0.001, (****) represents a p-value <0.0001, error bars represent the standard error of the mean (SEM). All experiments were independently performed at least twice.

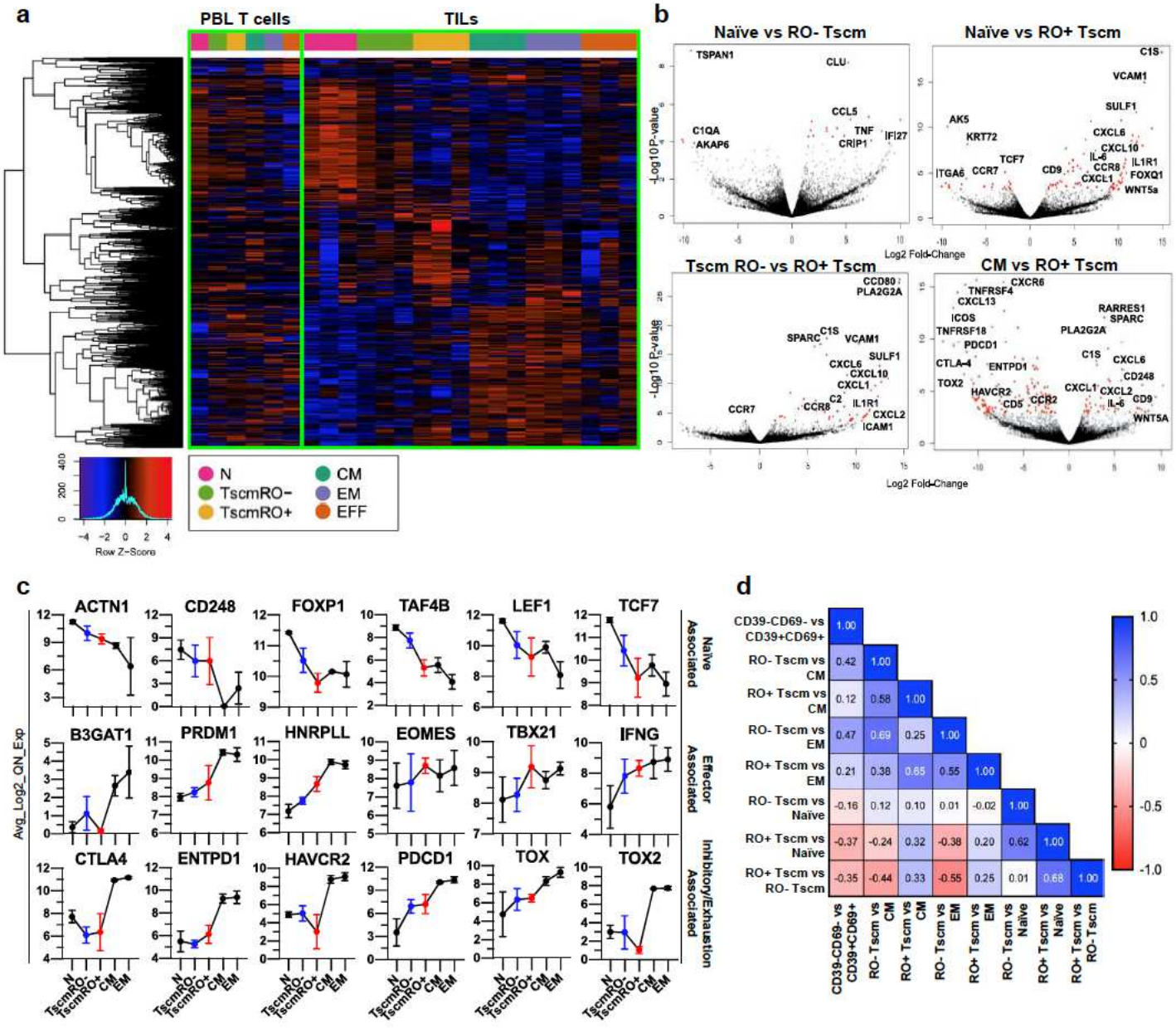

Figure 5

CD45RO+ Tscm TILs are transcriptionally intermediate between CD45ROTscm-like TILs and CM TILs, and express features associated with successful immunotherapy. (a) Bulk RNAseq DE gene expression heatmap showing DE gene results of sorted T cell differentiation subsets (FDR <=10%). Clustering was performed on the genes (rows). Reference PBL T cell subsets to the left, three different patient TILs for each T cell subset to the right. (b) Volcano plots showing significantly different genes (FDR <=10%) when comparing TIL differentiation subsets. (c) Gene expression trends for Naive (N), RO- Tscm, RO+ Tscm, CM, and EM subsets. Average quantile normalized expression for selected genes across cell types are shown. Error bars indicate the standard error. Row 1= Naive associated genes. Row 2= effector associated. Row 3= Inhibitory/exhaustion associated. (d) Heatmap displaying results of differential gene expression analysis using the Spearman Correlation to compare CD39-CD69- vs CD39+CD69+ expanded TILs (Krishna et al.14) to our RNAseq differentiation TIL subset comparisons.

Supplementary Files

This is a list of supplementary files associated with this preprint. Click to download.

- SupplementalFigure1.pdf
- SupplementalFigure2.pdf
- SupplementalFigure3.pdf
- SupplementalFigure4.pdf
- SupplementalFigure5.pdf